NCSX MAGNETIC CONFIGURATION FLEXIBILITY AND ROBUSTNESS

N. POMPHREY,[a]* A. BOOZER,[b] A. BROOKS,[a] R. HATCHER,[a] S. P. HIRSHMAN,[c] S. HUDSON,[a] L. P. KU,[a] E. A. LAZARUS,[c] H. MYNICK,[a] D. MONTICELLO,[a] M. REDI,[a] A. REIMAN,[a] M. C. ZARNSTORFF,[a] and I. ZATZ[a]

[a]*Princeton Plasma Physics Laboratory, Princeton, New Jersey 08540*
[b]*Columbia University, New York, New York 10027*
[c]*Oak Ridge National Laboratory, Oak Ridge, Tennessee 37831*

Received February 17, 2006
Accepted for Publication March 30, 2006

The National Compact Stellarator Experiment (NCSX) will study the physics of low–aspect ratio, high-β, quasi-axisymmetric stellarators. To achieve the scientific goals of the NCSX mission, the device must be capable of supporting a wide range of variations in plasma configuration about a reference baseline equilibrium. We demonstrate the flexibility of NCSX coils to support such configuration variations and demonstrate the robustness of performance of NCSX plasmas about reference design values of the plasma current I_p, β, and profile shapes. The robustness and flexibility calculations make use of free-boundary plasma equilibrium constructions using a combination of nonaxisymmetric modular coils and axisymmetric toroidal and poloidal field coils. The primary computational tool for the studies is STELLOPT, a free-boundary optimization code that varies coil currents to target configurations with specific physics properties.

KEYWORDS: *stellarator, design, flexibility*

I. INTRODUCTION

To achieve the scientific goals of the National Compact Stellarator Experiment (NCSX) mission, the NCSX device must be capable of supporting a range of variations in plasma configuration about the reference baseline equilibrium. We present a number of numerical calculations that demonstrate this ability:

1. an investigation of plasma performance as β and I_p are varied with fixed profile shape. Stable configurations with low effective helical ripple ε_h are found over a wide region of the I_p-β plane, with a stable path from a vacuum state to a full-current high-β configuration with $\beta > 5.0\%$.

2. an examination of plasma performance when plasma profiles are varied about reference forms at fixed I_p and β. A wide range of configurations is found whose β limits exceed 3.0% and that have good quasi-axisymmetry, including configurations with finite current at the plasma edge.

3. an examination of the ability to control the external transform $\iota_{ext}(s)$ by varying coil currents while constraining the toroidal field and plasma current to be constant. Substantial changes in $\iota(s)$ can be achieved, demonstrating an important control knob for transport and stability experiments on NCSX.

4. a demonstration of the ability to control the degree of quasi-axisymmetry while maintaining plasma stability. This provides a means to systematically explore the role of quasi-axisymmetry in improving the transport properties of stellarator plasmas.

5. a demonstration of the use of STELLOPT in defining experiments that elucidate the role of three-dimensional (3-D) shape stabilization in setting β limits separately for kink and ballooning modes.

Figure 1 shows a top view of the modular coil set M45 used for the flexibility and robustness studies. There are six coils in each of the three periods of the machine. Stellarator symmetry implies that within any given period only three coil currents are independent. The independent coils are labeled 1, 2, and 3. Stellarator-symmetric partners are labeled with prime superscripts. The same numbering convention will be used to identify the coils

*E-mail: pomphrey@pppl.gov

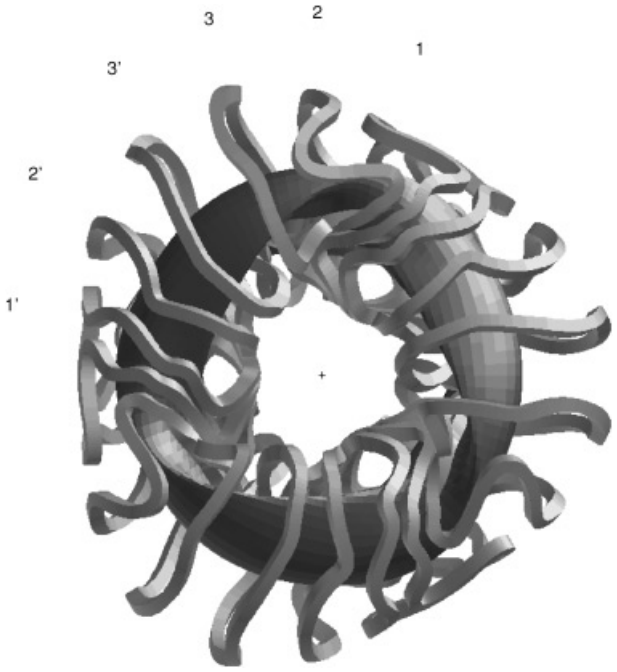

Fig. 1. Modular coil set M45 used for flexibility and robustness studies. Integers 1, 2, and 3 label the three coils within each period whose coil currents are allowed to vary independently of one another. Coil k' is the stellarator symmetric partner of coil k.

when presenting coil current solutions in our flexibility studies.

The three modular coil currents are allowed to vary independently; thus, the mean (toroidally averaged) toroidal magnetic field at a given radius will also vary. For systematic experiments it is advantageous to separate the provision of external transform by 3-D shaping from provision by changes in the average toroidal field (TF). In principle, the average toroidal field can be constrained to be a constant value by varying only two linear combinations of the three modular coil currents. However, this leads to a considerable reduction in flexibility to control the external transform. To avoid such a reduction in flexibility, NCSX includes an auxiliary TF coil system in which the TF coil current is allowed to vary together with the three modular coil currents in such a way that the mean TF field remains constant. The TF coil system is composed of 18 coils connected in series, capable of providing ± 0.5 T at radius $R = 1.4$ m.

A system of six axisymmetric poloidal field (PF) currents is included for additional flexibility (see Fig. 2). Coil PF6 is positioned to give a high-quality dipole (vertical) field in the plasma region. PF5 is positioned so that, in combination with PF6, a high-quality quadrupole field is produced. Coils PF4 and PF3 produce, in combination with PF5 and PF6, hexapole and octapole fields, respectively. Coils PF1 and PF2 are the primary ohmic heating

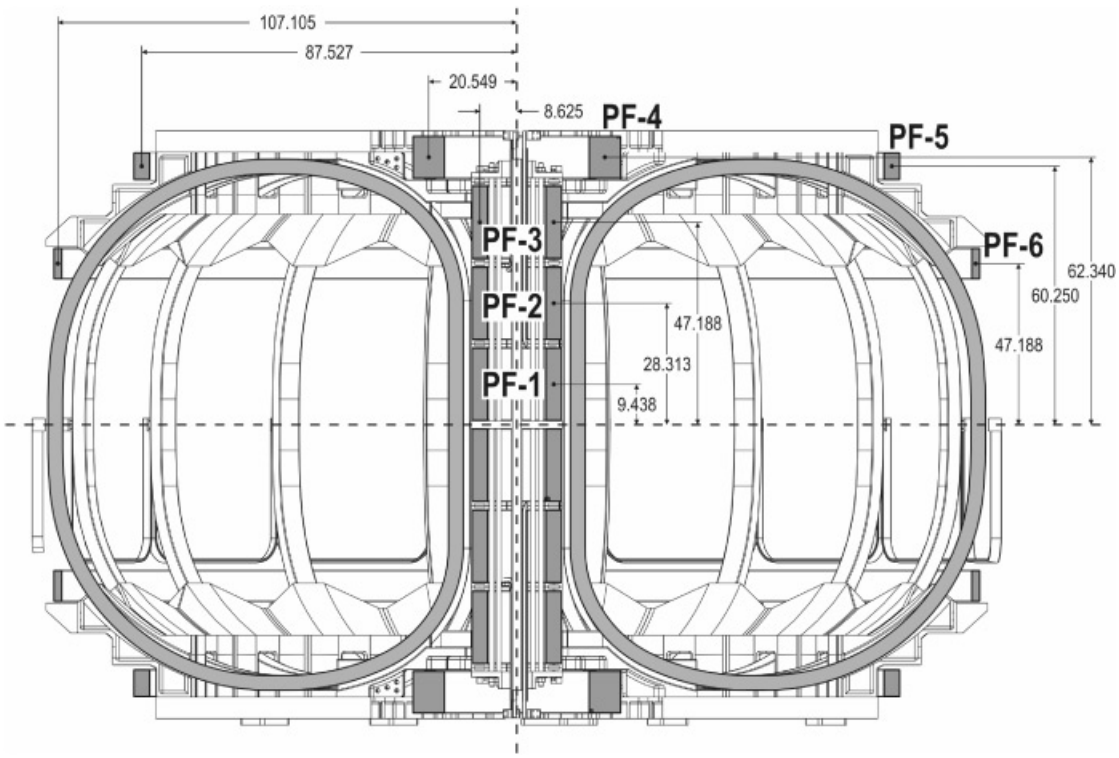

Fig. 2. PF coil geometry. PF3 through PF6 provide additional flexibility for the accomplishment of the physics mission.

TABLE I

Coil Current Limits (kA-turns) per Coil for Each of the Coil Systems*

M1 (kA-turns)	M2 (kA-turns)	M3 (kA-turns)	TF (kA-turns)	PF3 (kA-turns)	PF4 (kA-turns)	PF5 (kA-turns)	PF6 (kA-turns)
864.0	864.0	864.0	±194.0	±1739.0	±1397.0	±182.0	±73.0

*M = modular, TF = toroidal field, PF = poloidal field. Plasma configurations produced in the flexibility studies have coil currents that lie within the given limits.

coils and play no role in the flexibility calculations. Table I shows coil current limits for each of the independent coil systems. Plasma configurations for all calculations are constrained to lie within these limits.

The primary computational tool for the flexibility studies is STELLOPT (Ref. 1), a VMEC-based free-boundary optimizer that varies coil currents to target configurations with specific physics properties, such as stability to kink and ballooning modes and good quasi-axisymmetry (QA). Essential code modules within STELLOPT include an equilibrium solver [VMEC (Ref. 2)], stability analysis codes [TERPSICHORE (Ref. 3) for kink modes and COBRA (Ref. 4) for ballooning modes], and a QA analyzer. For the calculations presented here, the QA-ness measure targeted in STELLOPT is either $\chi^2_{Bmn} = \Sigma' B^2_{mn}/B^2_{00}$, where the B_{mn} are Fourier components of the magnetic field analyzed on the $s = 0.3$, 0.5, and 0.8 magnetic surfaces evaluated in Boozer magnetic coordinates, with the summation taken over modes with $n > 0$, or ε_h, the effective helical ripple, calculated by the NEO code module.[5] The targeted stability measures are $\chi^2_K = \lambda^2_{Kn=1} + \lambda^2_{Kn=0}$ (the square of the unstable eigenvalue of the dominant kink instability for the $n = 1$ and $n = 0$ kink families), and $\chi^2_B = \Sigma\lambda^2_B$ (the sum of squares of the maximum ballooning eigenvalue on any of the 49 magnetic surfaces used in the VMEC equilibrium calculation). All optimized equilibria are constrained to be tangent at some point to the plasma-facing-component first wall.

A requirement for the design of M45 coils[1,6] was that the coils should support a free-boundary equilibrium that reproduces the physics properties of the reference li383 S3 plasma configuration (S3 definition: $I_p = 174$ kA, $B_T = 1.7$ T at $R = 1.4$ m, with bootstrap consistency between current and pressure profiles, stable to kink and ballooning modes at $\beta > 4.2\%$, and good quasi-axisymmetry with effective helical ripple $\varepsilon_h \sim 0.5\%$ at $s = 0.5$). The reference profiles and reference M45 S3 plasma shape are shown in Figs. 3 and 4. Coil currents that produce S3 are presented in Table II. A summary of the shape and physics parameters for the kink and ballooning stable reference S3 state is given in Table III.

The S3 configuration defines a single point in the operating space of NCSX. In the following sections we address the following questions on robustness and performance: Using the M45 coil set,

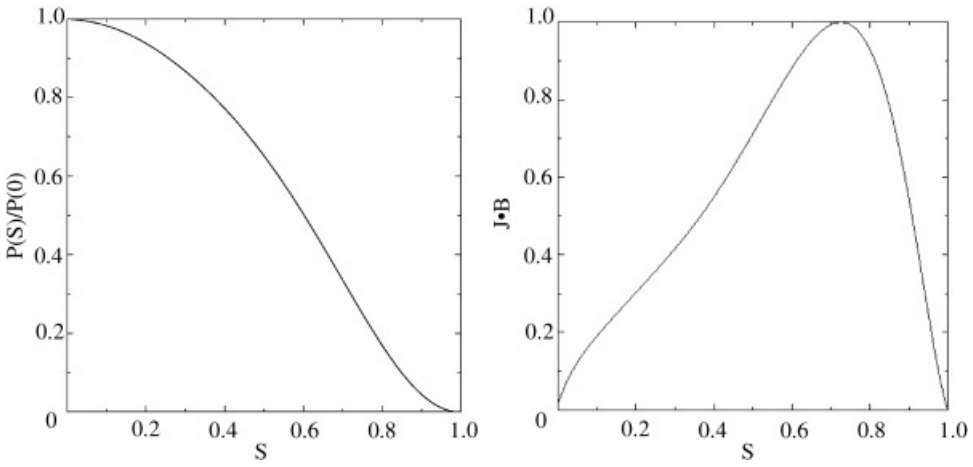

Fig. 3. Baseline reference pressure (P) and current ($J \cdot B$) profiles as a function of normalized toroidal flux s.

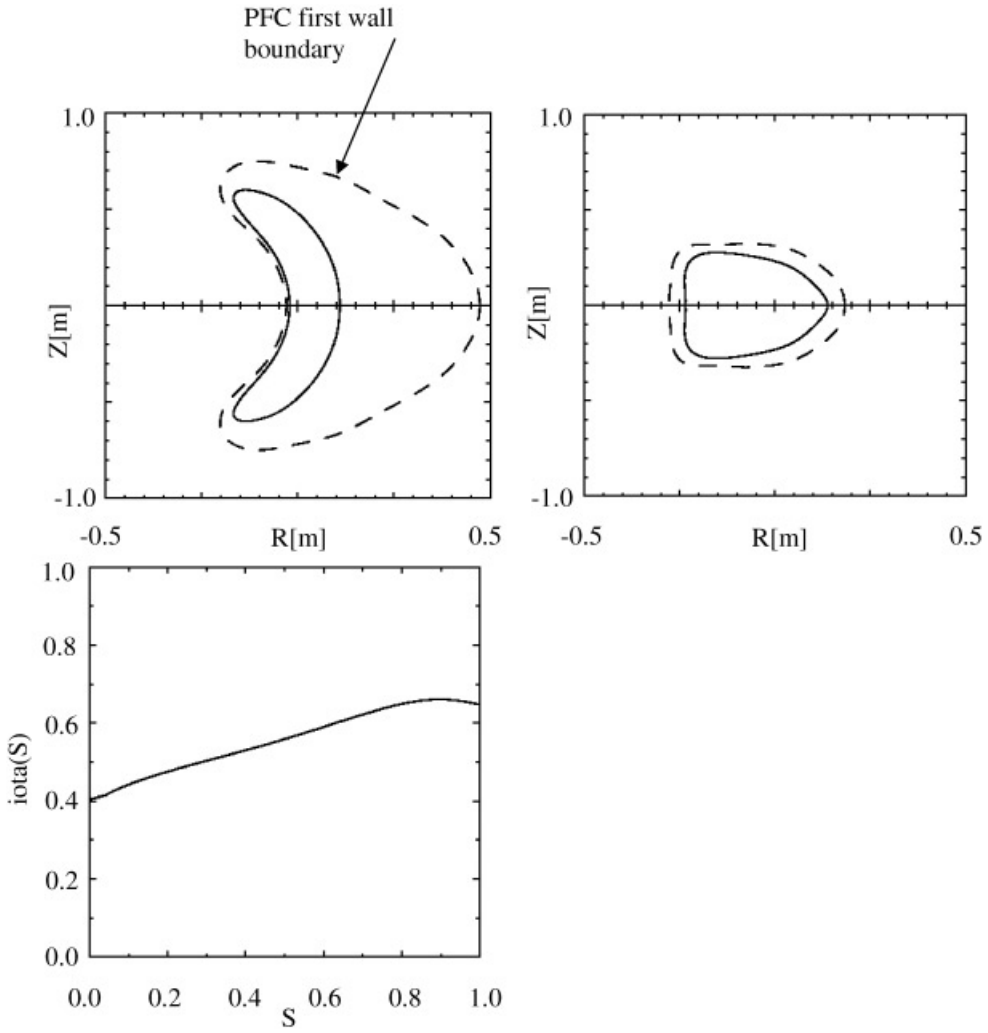

Fig. 4. Cross sections of plasma shape for reference S3 configurations at bean ($v = 0$) and bullet ($v = 0.5$) cross sections. Also, rotational transform as a function of normalized toroidal flux s.

1. How does the plasma performance change as currents and profiles are changed from the reference?

2. Is the operating space for configurations with adequate performance characteristics wide enough to allow fulfillment of the NCSX mission?

II. ROBUSTNESS OF PLASMA PERFORMANCE WITH RESPECT TO CHANGE IN COIL CURRENT

Whereas in later sections we use STELLOPT to find coil currents that support configurations with targeted physics properties, allowing several coil currents to vary,

TABLE II

Coil Currents for Reference M45 S3 State Using Plasma Profiles Shown in Fig. 2*

M1 (kA-turns)	M2 (kA-turns)	M3 (kA-turns)	TF (kA-turns)	PF3 (kA-turns)	PF4 (kA-turns)	PF5 (kA-turns)	PF6 (kA-turns)
694.2	654.6	551.1	27.8	1524.2	1180.0	95.2	−2.3

*$I_p = 174$ kA, $B_T = 1.7$ T, $\beta = 4.1\%$. Currents in ohmic coils PF1 and PF2 are zero.

TABLE III

Shape and Physics Parameters for Kink and Ballooning Stable Reference S3 Plasma Configuration

I_p (kA)	B_T (T)	R (m)	A	β (%)	$\varepsilon_h(s=0.5)$ (%)	$\iota(0)$	$\iota(1)$	ι_{max}
174	1.70	1.40	4.37	4.1	0.45	0.40	0.65	0.66

here we investigate the sensitivity of plasma shape and performance to legislated small changes in coil current using fixed plasma profiles.

Eight perturbations of the reference M45 S3 configuration were induced by separately incrementing each of the coil currents required to produce S3 (the currents shown in Table II) by 5% of the maximum current allowed for that coil. A ninth perturbation was defined by incrementing the plasma current by 5% of the reference S3 value. Free-boundary equilibria were calculated for each of these coil current perturbations at fixed toroidal flux, and the changes in selected plasma parameters are noted in Table IV.

The small changes in $R_{\max/\min}$ and $Z_{\max}$ at any toroidal angle that result from perturbing the coil currents imply that the plasma shape is robust with respect to the coil current changes. The neoclassical transport measure ε_h is also well preserved. In some cases a change in stability of either kink or ballooning modes is observed. The reason for the change in stability is the following: The optimizer that produced the reference configuration uses a heavyside cost function measure of stability with $\chi_K^2 = \lambda_K^2 > 0$ for unstable kink eigenvalues λ_K, while $\chi_K^2 = 0$ for a kink-stable configuration. Since the total χ^2 summed over all physics measures is minimized, optimum configurations are *marginally stable* to kink and ballooning modes. Perturbations of optimum configurations produced in this way are typically destabilized. As will be shown in later sections, the heavyside cost function feature of STELLOPT can be exploited to design experiments to test 3-D effects on β limits at low beta. The small changes in shape and parameters produced by arbitrary coil current perturbations of the optimized S3 configuration imply nothing as to the ability to derive configurations with properties very different from those of S3. We will show in later sections that NCSX flexibility is considerable if the correct coil current perturbations are used.

In the following sections, we investigate the performance of plasmas whose profiles and/or beta and net toroidal current differ from their reference forms and/or values. Coil currents are allowed to vary in such a way

TABLE IV

Effect on Plasma Parameters of Perturbing the S3 State by Incrementing the Modular Coil Current (M), Toroidal Field Coil Current (TF), Poloidal Field Coil Current (PF), and Plasma Current (I_p) by 5% of the Maximum Allowed Current*

	Perturbed Circuit								
	M1	M2	M3	TF	PF3	PF4	PF5	PF6	I_p
ΔI (kA turns)	+43.2	+43.2	+43.2	+9.7	+87.0	+69.9	+9.1	+3.7	+8.7
$\Delta R_{\max}$ (cm)	−0.3	−0.5	−2.2	−1.4	−0.0	−0.2	−0.6	−0.1	−0.7
$\Delta R_{\min}$ (cm)	+0.2	+0.3	+0.3	+0.8	−0.0	−0.2	−0.2	−0.0	−0.1
$\Delta Z_{\max}$ (cm)	−1.5	−0.7	+0.0	−1.4	−0.1	−0.1	+0.1	+0.1	−0.2
ΔA	+0.05	+0.05	+0.05	+0.04	+0.00	−0.00	−0.01	−0.00	+0.00
$\Delta\beta$ (%)	−0.18	−0.47	−0.19	−0.13	−0.00	−0.01	−0.01	−0.00	+0.00
$\Delta\iota(0)$	+0.005	+0.005	−0.004	−0.011	+0.001	+0.002	+0.002	+0.000	−0.000
$\Delta\iota(1)$	+0.005	−0.001	−0.008	−0.016	+0.000	−0.001	−0.004	−0.001	+0.019
ΔRB_T (T-m)	+0.05	+0.05	+0.05	+0.03	+0.00	+0.00	+0.00	−0.001	+0.00
$\Delta\text{kink}_{(n=0)}$	S→S↓	S→S	S→U	S→U	S→S	S→S	S→S	S→S	S→U
$\Delta\text{kink}_{(n=1)}$	S→S↓	S→S	S→U	S→U	S→S	S→S	S→S	S→S	S→U
$\Delta\text{ball}_{(n=\infty)}$	S→U	S→S↑	S→S↓	S→S↑	S→S	S→S	S→S	S→S	S→U
$\Delta\varepsilon_h$ (%)	+0.08	−0.02	+0.12	−0.02	−0.01	−0.02	−0.03	−0.01	−0.01

*$\Delta R_{\max/\min}$ is the change in the maximum/minimum plasma radius at any toroidal angle; $\Delta Z_{\max}$ is the change in the maximum plasma height at $v = 0$ (bean) cross section; ΔA is the change in the plasma aspect ratio; $\Delta\beta$ is the change in the plasma beta; $\Delta\iota(0)$ and $\Delta\iota(1)$ are the changes in the axis and edge values of the total rotational transform; ΔRB_T is the change in the radius times the toroidal magnetic field, evaluated at $R = 1.4$ m; $\Delta kink_{(n=0,1)}$ refers to the change in stability of the $n = 0$ and $n = 1$ families of kink modes (S denotes stable, S↑ denotes an increase in the stability margin compared with the reference case, and S↓ denotes a decrease in the stability margin; U denotes unstable); $\Delta ball_{(n=\infty)}$ refers to the change in stability of the ballooning modes; and $\Delta\varepsilon_h$ is the change in effective helical ripple evaluated at the $s = 0.5$ surface.

that χ^2_{Bmn} $(n \neq 0)$ is minimized while kink and ballooning stability are enforced. Plasmas are constrained to be limited by the first-wall boundary. We show that stable plasmas with good quasi-axisymmetry can be obtained for a wide range of assumed plasma conditions.

III. ROBUSTNESS OF PERFORMANCE AS β AND I_p ARE VARIED

In Ref. 7, discharge simulations are presented as a sequence of free-boundary equilibria corresponding to the "evolution" of an NCSX plasma from a particular S1 state where $\beta = 0.0\%$ to a final S3 state where $\beta > 4\%$. Pressure profile evolution is consistent with a one-dimensional transport model. The evolution from initial to final states can be represented as a curve on an I_p-β plane. Each point on the curve is associated with a particular profile of plasma current and pressure.

In this section, we explore the performance of NCSX plasmas for a wide range of values of β and I_p using fixed reference profiles—the S3 profiles of current and pressure shown in Fig. 3. In each case coil currents were varied to produce shape deformations of the plasma that lead to the minimization of a linear combination of χ^2_{Bmn} and the (square of the) growth rates for kink and ballooning modes. The average toroidal field was constrained to be constant, with $B_T = 1.7$ T at $R = 1.4$ m. Plasmas were constrained to be limited by the first-wall boundary.

Results are presented in Table V. In each block is listed the kink and ballooning mode stability characteristics

TABLE V

NCSX Plasma Performance for a Wide Range of β and I_p Values*

I_p (kA)	β (%)					
	0.0	1.0	2.0	3.0	4.0	5.0
0	Kink: N/A Balloon: N/A ε_h (%) = 0.33 0.79 S1 1.96	Kink: N/A Balloon: S ε_h (%) = 0.37 0.89 2.02	Kink: N/A Balloon: S ε_h (%) = 0.37 0.14 1.85	Kink: N/A Balloon: U	Kink: N/A Balloon: U	CASES NOT STUDIED
44	Kink: S Balloon: N/A ε_h (%) = 0.30 0.77 1.79	Kink: S Balloon: S ε_h (%) = 0.29 0.68 1.52	Kink: S Balloon: S ε_h (%) = 0.31 0.67 1.58	Kink: S Balloon: S ε_h (%) = 0.30 0.61 1.43	Kink: S Balloon: S ε_h (%) = 0.37 0.71 1.63	
87.5	Kink: S Balloon: N/A ε_h (%) = 0.27 0.71 1.64	Kink: S Balloon: S ε_h (%) = 0.28 0.65 1.51	Kink: S Balloon: S ε_h (%) = 0.26 0.51 1.22	Kink: S Balloon: S ε_h (%) = 0.39 0.72 1.58	Kink: S Balloon: S ε_h (%) = 0.31 0.60 1.60	
131	Kink: S Balloon: N/A ε_h (%) = 0.23 0.52 1.33	Kink: S Balloon: S ε_h (%) = 0.25 0.46 1.06	Kink: S Balloon: S ε_h (%) = 0.23 0.42 1.06	Kink: S Balloon: S ε_h (%) = 0.29 0.41 0.95	Kink: S Balloon: S ε_h (%) = 0.23 0.45 1.23	
174	Kink: S Balloon: N/A ε_h (%) = 0.19 0.37 S2 0.93	Kink: S Balloon: S ε_h (%) = 0.21 0.39 0.95	Kink: S Balloon: S ε_h (%) = 0.18 0.36 0.82	Kink: S Balloon: S ε_h (%) = 0.19 0.40 1.04	Kink: S Balloon: S ε_h (%) = 0.21 0.45 S3 1.15	Kink: S Balloon: S ε_h (%) = 0.56 0.92 2.15

*In all but the two cases shown in the shaded blocks, optimized configurations were found to be stable (S) to kink and ballooning modes with good quasi-axisymmetry. Only $I_p = 0$ kA, $\beta = 3\%$ and $I_p = 0$ kA, $\beta = 4\%$ were unstable (U) to ballooning modes. The effective helical ripple strength ε_h is tabulated for the $s = 0.3$, 0.5, and 0.8 magnetic surfaces. It is small over the entire range of the table. A stable configuration was obtained at $I_p = 174$ kA, $\beta = 5\%$.

of the optimized configuration, as well as the effective helical ripple strength ε_h (%), evaluated on the $s = 0.3$, 0.5, and 0.8 magnetic surfaces. Stable free-boundary equilibria were found for nearly every case in the calculated I_p-β plane. All equilibria were stable to kink modes; nearly all equilibria were stable to ballooning modes. For $I_p =$ 174 kA the free-boundary equilibrium with $\beta = 5.0\%$ was stable to both ballooning and kink modes. This β value is substantially higher than the reference li383 fixed-boundary β limit. [A full exploration of the maximum β limit using the M45 coils has not yet been made; however, a kink-stable configuration was found with $\beta =$ 6.0% and $\varepsilon_h = 0.8\%$ at s = 0.5 using the standard (unoptimized) S3 profiles. Ballooning modes for this $\beta =$ 6% configuration were unstable on only two adjacent magnetic surfaces near the edge of the plasma.] Two cases in Table V were unstable to ballooning modes. These cases (shaded boxes) are $I_p = 0$ kA, $\beta = 3.0\%$ and $I_p = 0$ kA, $\beta = 4.0\%$. With regard to QA-ness, $\varepsilon_h < 0.5\%$ at $s = 0.5$, typically, and ε_h never exceeds 1.0% at $s = 0.5$. As discussed in Ref. 8, it is expected that for this magnitude of ripple amplitude, and with standard conditions of plasma temperature and density, the helical ripple transport will be small compared with axisymmetric neoclassical transport.

Using reference profiles, we conclude there is a substantial region of stability with good QA-ness in the I_p-β plane.

The maximum difference between the coil currents for any equilibrium state in the I_p-β scan of Table V and the reference M45 S3 state is presented in Table VI. For the modular coil currents the variation is less than 10% from the nominal S3 currents (Table II). The variation in poloidal field coil current is ~100%. Plots of coil current versus beta, as a fraction of allowed current, are shown in Fig. 5 for the diagonal sequence $I_p \propto \beta$ connecting the vacuum state, S1, and the reference full-current, high-beta state, S3. Coil currents for this sequence, as well as for all cases shown in Table V, are within the allowables range.

An overlay of plasma boundaries and calculated iota profiles for a subset of stable equilibria from the I_p-β scan are presented in Fig. 6. A wide range of plasma boundary shapes and iota profiles is seen, including a substantial variation in magnetic shear, $d\iota/ds$. These data show the possibility of designing experiments to investigate shear stabilization of neoclassical tearing modes. Later, in Sec. VI, we show how the ability to control $\iota(s)$ at fixed I_p and β using the external magnetic fields allows the design of experiments to investigate 3-D shape stabilization of external kink modes.

IV. ROBUSTNESS OF PERFORMANCE AS PLASMA PROFILES ARE VARIED

For the results presented so far, the current and pressure profiles have had the same form as the reference li383 profiles. Now we investigate the effect on plasma performance of choosing plasma profiles that are different from the reference profiles. First, we examine the performance of plasmas supported by NCSX coils for a range of current profiles, fixing the pressure profile equal to the reference form shown in Fig. 3. The effect of varying the current profile in the core region of the plasma is considered separately from its effect in the edge region. In another set of experiments, the effect of varying the pressure profile is considered, with the current profile held fixed equal to its reference form, also shown in Fig. 3. We show that good plasma performance is obtained for a wide range of current and pressure profiles. The results allay concern that the optimization methods used for designing the plasma configuration and coil system may have produced only a narrow operating space of good performance plasmas.

IV.A. Variation of the Current Profile in the Core Region

Here we examine the performance of plasmas supported by NCSX coils for current profiles that differ from the reference form mainly in the core region. A one-parameter family of current profiles J_α is conveniently defined by

$$J_\alpha(s) = (1 - \alpha)J^{ref}(s) + \alpha J^{peaked}(s) \ , \qquad (1)$$

TABLE VI

Coil Current Variation for the I_p-β Scan Results*

ΔI_{M1} (kA-turns)	ΔI_{M2} (kA-turns)	ΔI_{M3} (kA-turns)	ΔI_{TF} (kA-turns)	ΔI_{PF3} (kA-turns)	ΔI_{PF4} (kA-turns)	ΔI_{PF5} (kA-turns)	ΔI_{PF6} (kA-turns)
+52 −38	+41 −12	+46 −27	+31 −46	+0 −1691	+0 −1627	+78 −222	+28 −36

*In each column is shown the maximum +/− variation in the current for coil k compared with the current required to support the S3 state.

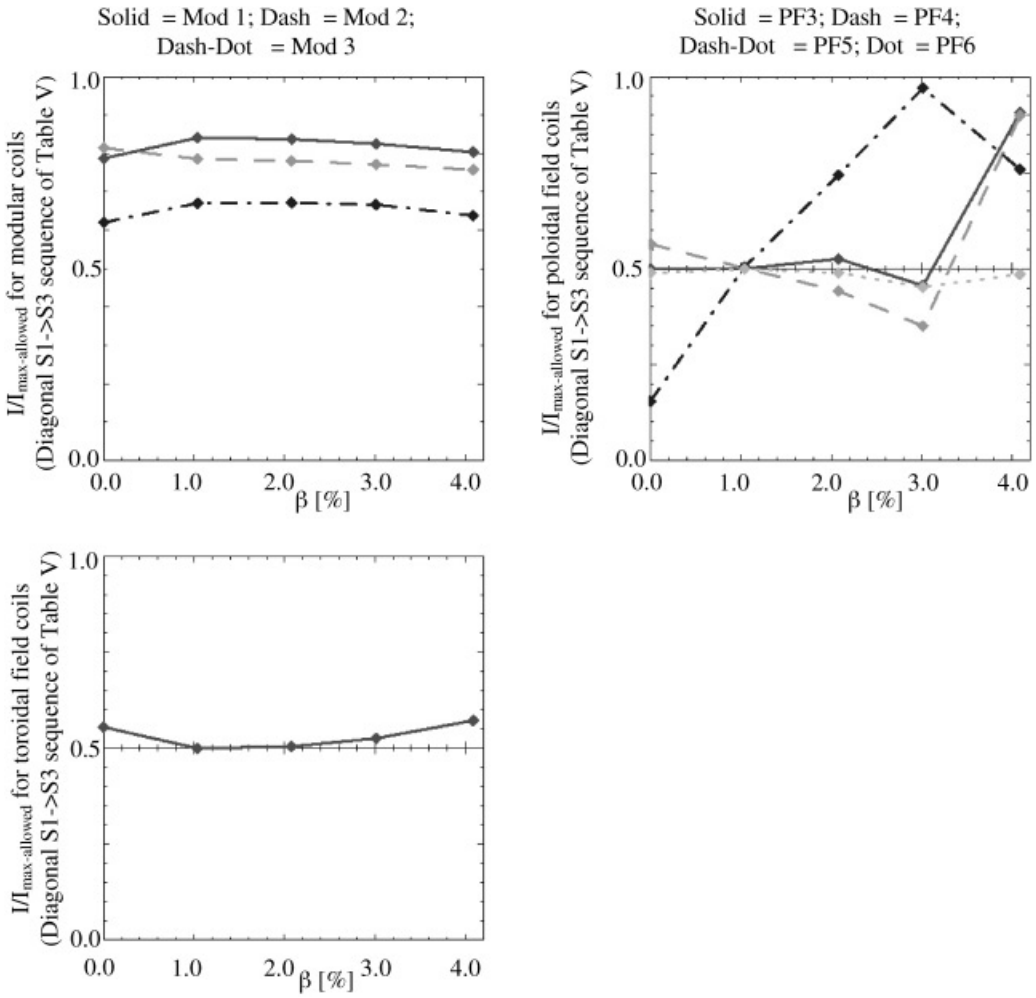

Fig. 5. Coil currents as fraction of allowable current per coil for the sequence $I_p \propto \beta$.

where $0 \leq \alpha \leq 1$ and $J(s)$ denotes the surface-averaged parallel current profile $\mathbf{J} \cdot \mathbf{B}$. As α ranges from zero to one, J_α undergoes a substantial change in shape, from the reference hollow current profile J^{ref} of Fig. 3 to a peaked current profile defined as $J^{peaked} = 1 - s^2$. A plot of the J_α for different α is shown in Fig. 7.

With $\alpha = 0.0$, $J_\alpha = J^{ref}$ and the plasma configuration is identical to the reference configuration. As discussed in Sec. III, the free-boundary β limit for these profiles is at least $\beta = 5.0\%$. For $\alpha > 0$ we execute a sequence of free-boundary optimizer runs, increasing α from 0.0 in steps of 0.1, to determine the range of values of α (i.e., range of current profiles) for which NCSX plasmas are stable at $\beta = 3.0\%$. For each run, the plasma current was held fixed at $I_p = 174$ kA, and the average toroidal field at $R = 1.4$ m is $B_T = 1.7$ T.

Table VII shows a summary of the kink and ballooning stability properties for the various optimized configurations, including values of the effective ripple ε_h. It is seen that current profiles with $0 \leq \alpha \leq 0.5$ are stable to kink and ballooning modes, with quasi-axisymmetry measure $\varepsilon_h < 0.5\%$ at $s = 0.5$. This wide range of stable profiles at $\beta = 3\%$ is the same as that presented at the Physics Validation Review.

Table VIII shows a summary of the coil current changes required to maintain stable equilibria while accommodating the profile changes. The current changes are small, with the maximum change in coil current occurring, as expected, for the limiting case $\alpha = 0.5$, where the optimizer has the most difficulty in stabilizing the plasma.

Figure 8 shows an overlay of plasma boundaries and calculated iota profiles for the α sequence of stable configurations. The variation in plasma boundary shape is seen to be very small; however, the variation in the shear of the iota profile is substantial. As α increases and current is added to the core region of the plasma, the axis value of iota increases. The edge iota, although unconstrained in the present optimization runs, remains nearly constant. The onset of instability as α is raised to $\alpha = 0.5$ may be correlated with a lack of adequate shear in the

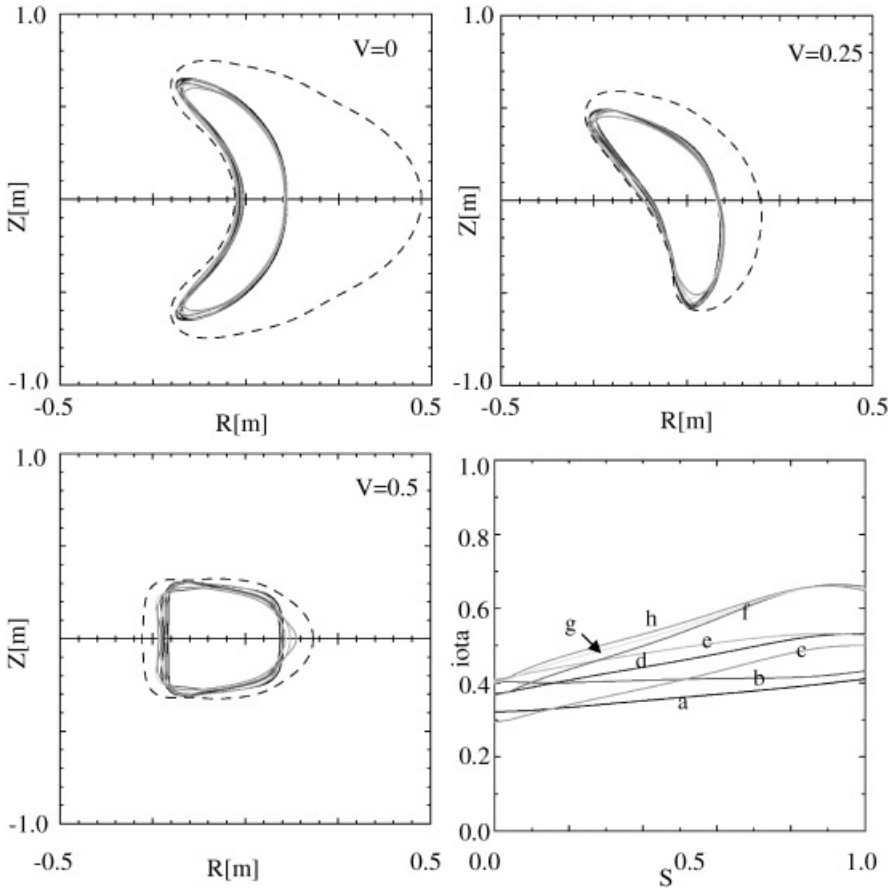

Fig. 6. Overlay of plasma boundaries and calculated iota profiles for various optimized equilibria from the I_p-β scan (Table V). The calculated iota profiles are (a) $I_p = 0$ kA, $\beta = 0\%$, (b) $I_p = 0$ kA, $\beta = 2\%$, (c) $I_p = 87.5$ kA, $\beta = 0\%$, (d) $I_p = 87.5$ kA, $\beta = 2\%$, (e) $I_p = 87.5$ kA, $\beta = 4\%$, (f) $I_p = 174$ kA, $\beta = 0\%$, (g) $I_p = 174$ kA, $\beta = 2\%$, and (h) $I_p = 174$ kA, $\beta = 4\%$. Note the wide range of iota profiles (shear and edge iota values) for which plasmas were found to be stable.

iota profile. On the other hand, we see from the $\iota(s)$ plots of the $I_p = 174$ kA, $\beta = 0$, 2, and 4% sequence of marginally stable equilibria shown in Fig. 6 that such an assumption may be presumptive. Further study is needed to confirm such a conclusion.

IV.B. Variation of the Current Profile in the Edge Region

We now explore the effect of varying the current profile in the edge region. In particular, we consider the family of current profiles J_δ, shown in Fig. 9, where

TABLE VII

Stability Properties and Effective Helical Ripple ε_h at $s = 0.3$, 0.5, and 0.8 for Current Profiles Parameterized by Peakedness Parameter α [see Eq. (1) and Fig. 7]*

α						
0.0	0.1	0.2	0.3	0.4	0.5	0.6
Kink: S Balloon: S ε_h (%) = 0.19 0.40 1.04	Kink: S Balloon: S ε_h (%) = 0.18 0.40 1.12	Kink: S Balloon: S ε_h (%) = 0.18 0.42 1.25	Kink: S Balloon: S ε_h (%) = 0.19 0.45 1.36	Kink: S Balloon: S ε_h (%) = 0.20 0.49 1.42	Kink: S Balloon: S ε_h (%) = 0.21 0.49 1.38	Kink: U

*All equilibria correspond to $I_p = 174$ kA, $\beta = 3.0\%$, with $B_T = 1.7$ T at $R = 1.4$ m. The stable range of α is $0 \leq \alpha \leq 0.5$.

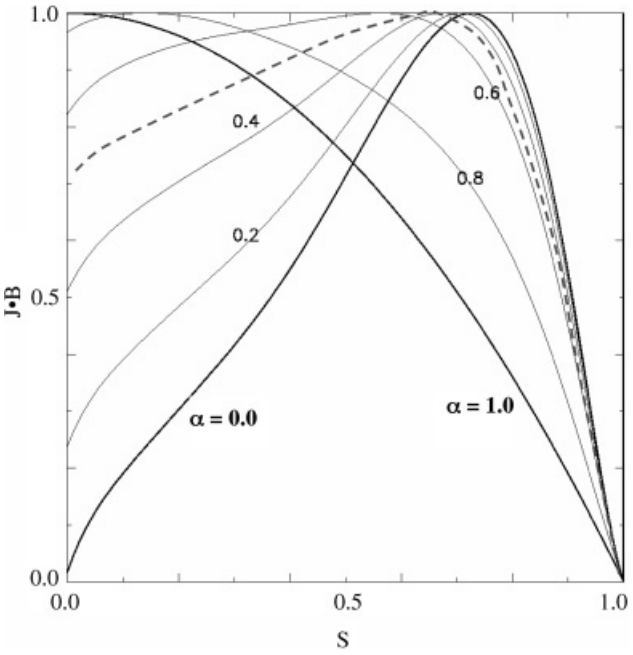

Fig. 7. A one-parameter family of current profiles that differ mainly in the core region. The stable range of current profiles is $0 \le \alpha \le 0.5$. The $\alpha = 0.5$ profile is shown as a dashed curve. For the stable range of α, the internal inductance ℓ_i of an equivalent tokamak with the same average elongation, triangularity, and aspect ratio ranges from 0.30 to 0.54.

$$J_\delta(s) \propto J^{ref}(s) + \delta J^{edge}(s) \ , \quad J^{edge}(s) = s^{10} \ . \quad (2)$$

Such a parameterization allows a sizeable current density near the plasma edge. The values of δ shown in Fig. 9 represent the magnitude of J_δ at the plasma edge relative to the maximum value of $J_\delta(s)$. δ varies from 0.0 to 0.5 in steps of 0.1.

Whereas in Sec. IV.A we considered free-boundary equilibrium reconstructions at $\beta = 3.0\%$, in this section we examine the stability characteristics of finite edge current free-boundary plasmas at $\beta = 5.0\%$, a value that exceeds the reference fixed-boundary β limit for li383.

Already the I_p-β scan presented in Table V has shown a stable configuration with $I_p = 174$ kA, $\beta = 5.0\%$. The coil currents for this $\delta = 0.0$ configuration are shown in Table IX. Using the same coil currents, free-boundary equilibria were calculated for each of the current profiles shown in Fig. 9. In each case $I_p = 174$ kA, $\beta = 5.0\%$, with $B_T = 1.7$ T at $R = 1.4$ m, and the pressure profile was fixed equal to the reference form. Remarkably, each current profile for the new calculated equilibrium is found to be stable to kink and ballooning modes.

The robust stability for the sequence of equilibria with different edge current densities can be understood in terms of the effect on the iota profile of adding successive current layers to the plasma edge region. Figure 10 shows overlays of the plasma boundaries and profiles of $\iota(s)$ for the equilibria with $\delta = 0.0$, 0.2, and 0.4. It should be noted that as more edge current is included, the shear $d\iota/ds$ in the edge region of the plasma is increased with no change in the edge iota. Such an increase in shear is known to be stabilizing for current-carrying stellarators.[9,10]

An increase in current density near the plasma edge is an expected consequence of a transition from *L*- to *H*-mode profiles. In view of the observations made above, there is an interesting possibility that such a transition will have beneficial effects on magnetohydrodynamic (MHD) stability. Future calculations should calculate β limits for realistic models of *H*-mode profiles in NCSX.

In Fig. 10 we present, for comparison, the plasma boundary and iota profile for the reference S3 equilibrium corresponding to $\beta = 4\%$, $\delta = 0.0$. It is interesting to observe that the edge iota values for the $\beta = 4$ and 5% equilibria are quite different; $\iota_{\max} \approx \frac{2}{3} = 0.67$ for the S3 equilibrium with $\beta = 4\%$, whereas $\iota_{\max} \approx \frac{3}{5} = 0.60$ for the $\beta = 5\%$ equilibria. It appears that the preferred shape for the $\beta = 5\%$ configuration is one that avoids having $\iota = \frac{3}{5}$ in the plasma region; STELLOPT adjusts the coil currents in such a way as to accommodate this preference. Similar observations have been made for configurations obtained in the I_p-β scan; for fixed β of 4.0%, if I_p is raised in small increments from 131 to 174 kA, configurations optimized for stability and quasi-axisymmetry have $\iota_{\max}$ values that change abruptly from 0.60 to 0.67. No intermediate values of $\iota_{\max}$ are found.

TABLE VIII

Coil Current Variation for the Current Profile Scans*

ΔI_{M1} (kA-turns)	ΔI_{M2} (kA-turns)	ΔI_{M3} (kA-turns)	ΔI_{TF} (kA-turns)	ΔI_{PF3} (kA-turns)	ΔI_{PF4} (kA-turns)	ΔI_{PF5} (kA-turns)	ΔI_{PF6} (kA-turns)
+26 −4	+5 −4	+3 −1	+4 −1	+0 −8	+0 −168	+8 −0	+1 −0

*In each column is shown the maximum +/− variation in the current for coil *k* compared with the current required to support the $\alpha = 0$ state.

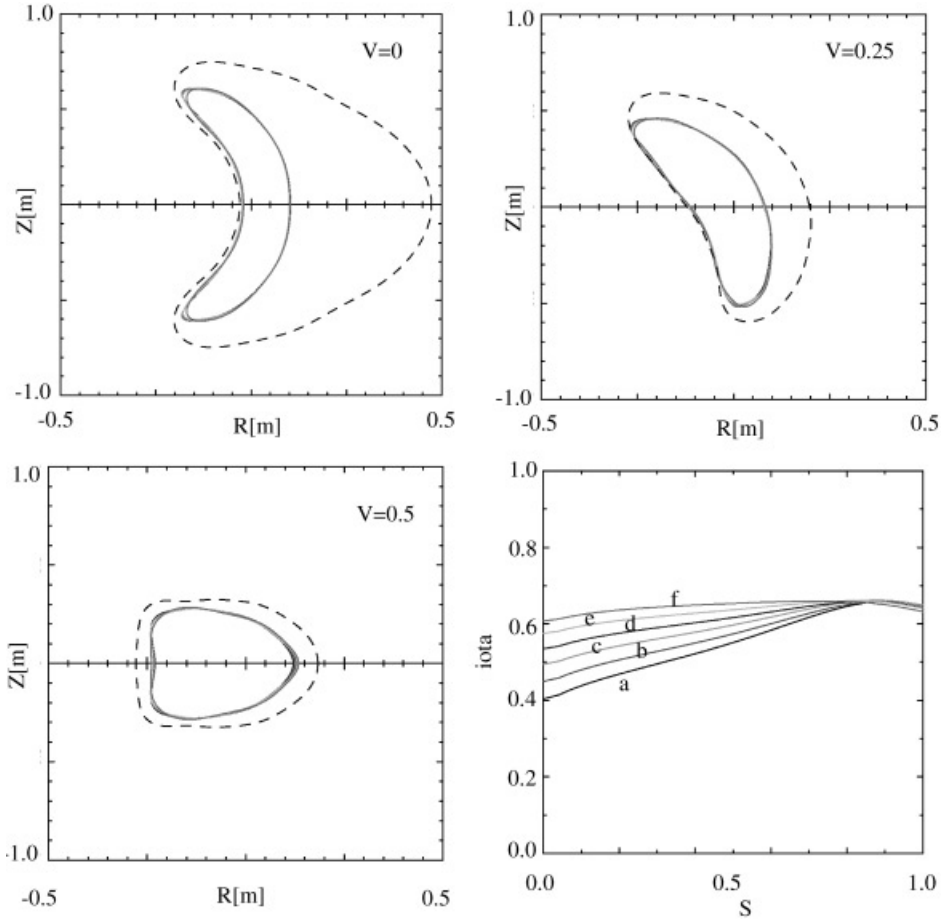

Fig. 8. Overlay of plasma boundaries for stable equilibria at $\beta = 3.0\%$ for the J_α sequence of current profiles (where $\mathbf{J}\cdot\mathbf{B}$ is varied in the core region). The calculated iota profiles are (a) $\alpha = 0.0$, (b) $\alpha = 0.1$, (c) $\alpha = 0.2$, (d) $\alpha = 0.3$, (e) $\alpha = 0.4$, and (f) $\alpha = 0.5$.

This appears to be due to the simultaneous optimization of stability and QA-ness. If the weighting of the QA contribution to the STELLOPT cost function is decreased while preserving the same weighting for the stability cost function, configurations with any chosen value of $\iota_{\max}$ between 0.60 and 0.67 are obtained using the edge ι control procedure discussed in Sec. V.

IV.C. Variation of the Pressure Profile

As another set of numerical experiments, we examine the performance of plasmas supported by NCSX coils for a range of pressure profiles. The current profile shape is held fixed equal to the reference form. First, a one-parameter family of pressure profiles is defined by

$$p_\gamma(s) = (1-\gamma)p^{ref}(s) + \gamma p^{peaked}(s) \ , \qquad (3)$$

where $0 < \gamma < 1$. As γ ranges from zero to one, p_γ undergoes a change from the (broad) reference pressure profile to a more peaked pressure profile, whose analytic dependence on toroidal flux is chosen to be $p^{peaked} \propto (1-s)^2$. This "peaked" form is a good fit with typical neutral beam injection–heated PBX-M discharge

TABLE IX

Coil Currents Corresponding to the Stable Configuration with $I_p = 174$ kA, $\beta = 5.0\%$ Presented in Table V*

M1 (kA-turns)	M2 (kA-turns)	M3 (kA-turns)	TF (kA-turns)	PF3 (kA-turns)	PF4 (kA-turns)	PF5 (kA-turns)	PF6 (kA-turns)
655.8	651.2	524.3	58.6	1230.3	447.9	79.9	−1.3

*These currents are used in free-boundary equilibrium reconstructions that vary the edge current density.

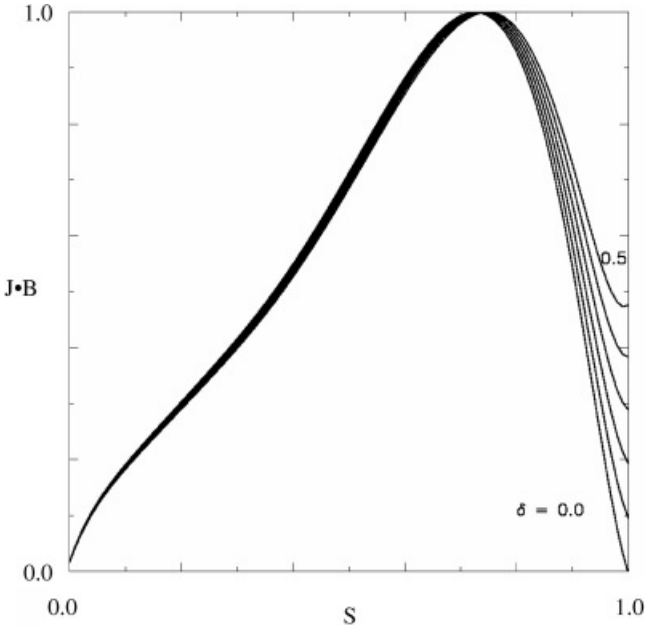

Fig. 9. Family of current profiles $J_\delta(s)$ that vary mainly in the edge region. Stability may be enhanced as the edge current builds due to an increase in the global shear.

profiles.[11] A plot of the p_γ for different values of γ is shown in Fig. 11. The p_γ profiles all have zero pressure gradient at the plasma edge, $s = 1$.

A sequence of free-boundary optimizer runs was executed at $\beta = 3.0\%$, increasing γ from 0.0 to 1.0 in steps of 0.2 to determine the range of pressure profiles for which NCSX plasmas supported by the designed coils are stable to ballooning and kink modes with optimized quasi-axisymmetry. As in Sec. IV.A, we chose $I_p = 174$ kA, $\beta = 3.0\%$ with $B_T = 1.7$ T at $R = 1.4$ m, making no attempt to optimize β by changing I_p from this reference value.

Table X summarizes the optimizer runs as the peakedness parameter γ is varied. For the given parameterization of $p(s)$, stable configurations with good quasi-axisymmetry ($\varepsilon_h < 0.5\%$ at $s = 0.5$) were found for all cases except $\gamma = 1.0$. For this case, we have found a stable configuration at $\beta = 2.5\%$. Figure 12 shows an overlay of the plasma boundaries and iota profiles for each of the stable optimized configurations with $\gamma \leq 0.8$. One sees little change in the optimized plasma shape for these changes in pressure profile. Table XI shows a summary of the coil current changes required to maintain the stable equilibria for the various pressure profiles. Consistent with the small plasma shape changes, the current changes are also small.

The effect on performance of including a finite edge pressure gradient was also investigated using a profile form defined by

$$p_{pedestal}(s) = p^{ref}(s) + cs^7(1 - s^3) \ , \qquad (4)$$

with coefficient c adjusted to give a desired edge pressure gradient. A sequence of optimizer runs was executed using pressure profiles of the form of Eq. (4). A configuration, stable at $\beta = 3\%$ and with good QA measure $\varepsilon_h = 0.56\%$, was obtained for the pedestal profile labeled in Fig. 11. For this profile, the chosen c gives $(dp/ds)/p_0|_{s=1} = -2.2$. The coil currents for this configuration were included in the data for Table XI.

The operating space of stable configurations with $\beta = 3.0\%$, including substantial variations in current and pressure profiles and good quasi-symmetry, appears to be broad. We also note that it should be possible to widen the operating space of stable profiles defined above by allowing the plasma current to vary in addition to the shape.

V. FLEXIBILITY TO CONTROL THE EXTERNAL TRANSFORM

We now demonstrate the capability of NCSX coils to effect substantial changes in the external field contribution to $\iota(s)$. The MHD stability of stellarator plasmas can depend critically on details of the iota profile, for example, on the location of the $\iota = 0.5$ magnetic surface. W7-AS experiments[12] demonstrate cases where stability depends not on the magnitude of the external transform ι_{ext} but on the ability to avoid $\iota = 0.5$ in the plasma and hence $q = 2$ global tearing modes. The reference S3 configuration for NCSX has $\iota(0) = 0.40$, $\iota(1) = 0.65$. A natural S1 "vacuum" configuration associated with S3, obtained by running STELLOPT with $I_p = 0$ kA, $\beta = 0\%$ and optimizing coil currents for QA transport with no constraints on iota, yields the configuration tabulated in Table V with $\iota(0) = 0.34$, $\iota(1) = 0.42 => \iota(s) < 0.5$ for all s values. Plasma evolution from this S1 state to the reference S3 implies passage through $\iota(1) = 0.5$. The results of Sec. III suggest that NCSX coil currents can be chosen to evolve in such a way that 3-D shaping of the plasma avoids the trigger of any kink mode (for example, evolution through states corresponding to the "diagonal" sequence in Table V where $\beta \propto I_p$). Nevertheless, it is important to have the ability to control the iota profile through external shaping so that $\iota(1) = 0.5$ can be avoided, if this is found to be necessary in the actual experiment. This capability is exploited in Ref. 7, where a "high-iota" start-up scenario is presented that avoids passage through $\iota(1) = 0.5$. The ability to control $\iota(s)$ is also a very useful control knob to aid the mapping of stable/unstable boundaries for NCSX.

V.A. Variation of $\iota(s)$ at Fixed Shear

Here we demonstrate the ability to raise and lower $\iota(s)$ while keeping the shear essentially constant. As a baseline plasma whose iota profile is to be changed, we chose the reference S3 state with $I_p = 174$ kA, $\beta = 4.2\%$

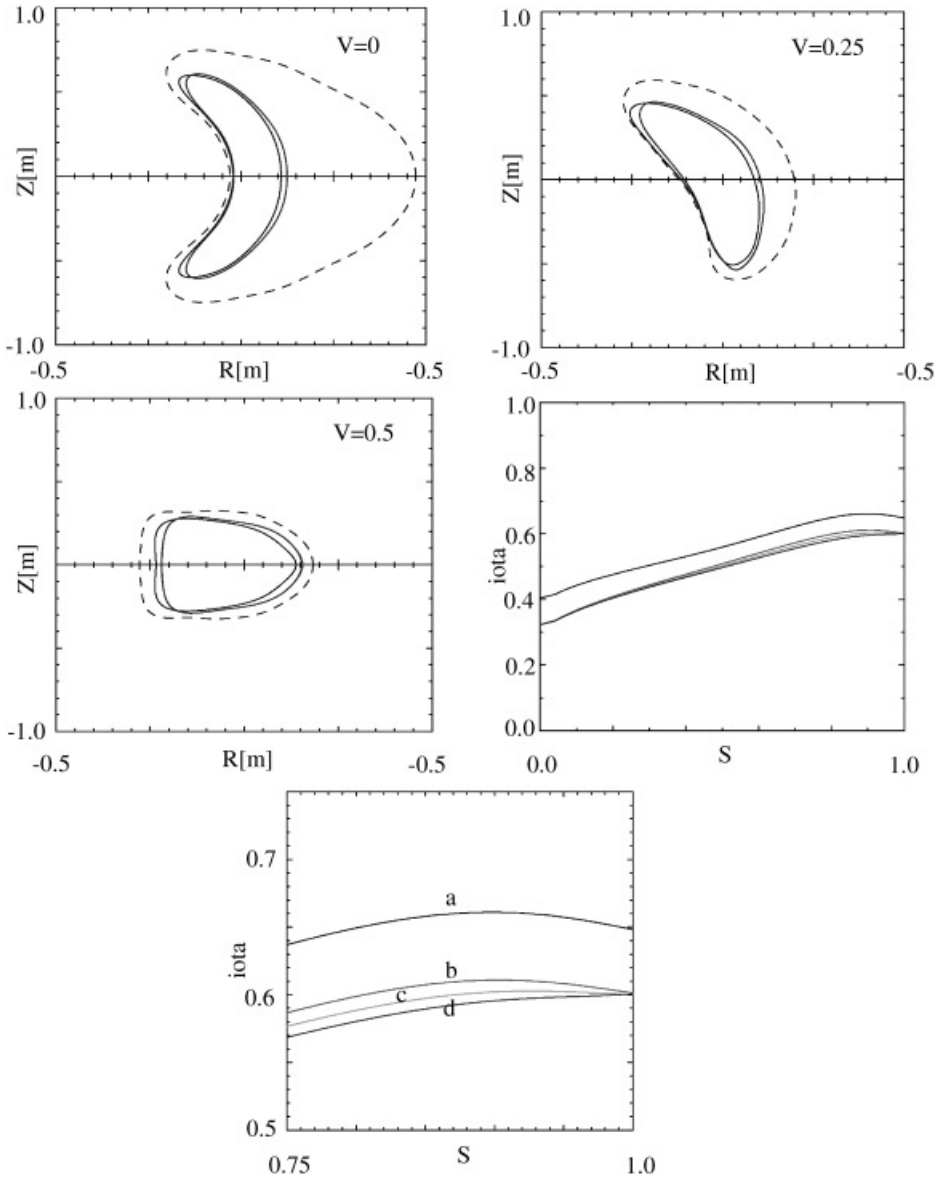

Fig. 10. Overlay of three plasma boundaries for stable equilibria at $\beta = 5\%$ with varying edge current densities ($\delta = 0.0$, 0.2, and 0.4). The coil currents are the same in all cases. The plasma boundaries vary little, but there is seen to be a difference with the plasma boundary for the reference S3 state with $\beta = 4\%$. Also shown are the $\iota(s)$ profiles (shown plotted in two frames, the second of which is a magnification of the first), from which the increase in edge shear is evident: (a) $\beta = 4\%$, $\delta = 0.0$ (S3 state), (b) $\beta = 5\%$, $\delta = 0.0$, (c) $\beta = 5\%$, $\delta = 0.2$, and (d) $\beta = 5\%$, $\delta = 0.4$.

and axis and edge iota values of $\iota(0) = 0.40$ and $\iota(1) = 0.65$, respectively. The choice of baseline plasma for the iota flexibility experiments is arbitrary, since in an actual experiment we may be interested in exploring the effects of changing the iota profile for a variety of plasma states. For the iota scan experiments we target desired changes in $\iota(0)$ and $\iota(1)$ relative to the baseline values and optimize χ^2_{Bmn}, making no attempt to stabilize the kink and ballooning modes; the goal here is to explore coil flexibility, not plasma performance. The plasma current is held fixed at $I_p = 174$ kA, and the toroidally averaged B_T is held constant at 1.7 T at $R = 1.4$ m. We seek to change $\iota(s)$ at fixed plasma current and toroidal field by 3-D shaping only. All configurations are further constrained by the first-wall poloidal field coil (PFC) boundary.

Figure 13 shows plasma boundaries and calculated iota profiles for cases where $\iota(0)$ and $\iota(1)$ were programmed to change by equal amounts so as to keep the shear constant. Substantial changes $\Delta\iota(s) \in [-0.2, +0.1]$ relative to the baseline are shown possible. The required

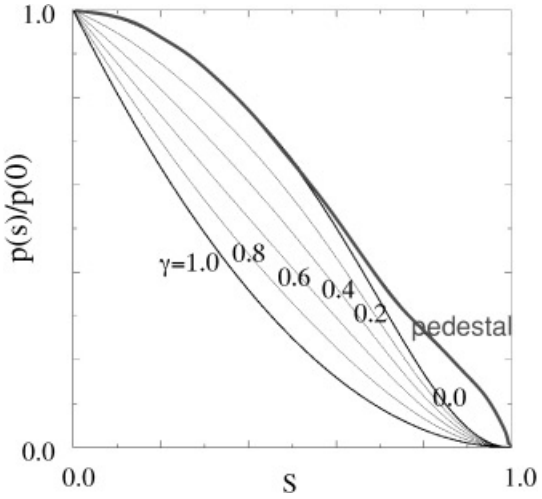

Fig. 11. The one-parameter family of pressure profiles P_γ, for which plasma performance is evaluated at $\beta = 3\%$. $\gamma = 0.0$ is the reference profile. Also shown is the edge pedestal profile, for which a stable configuration was also obtained at $\beta = 3\%$.

coil currents to effect these changes are shown in Table XII. We note the range of shapes required to produce the target iota profiles and the correlation of shape with the limits on the range of $\Delta\iota(s)$. For $\Delta\iota(s) = +0.1$ [curves labeled (d) in Fig. 13], the plasma cross section at the $v = 0.5$ symmetry plane has an extremely pointed nose region. Not only does this present numerical difficulties for the VMEC equilibrium solver, but one must eventually worry about the viability of such a shape on physics grounds, for example, on account of neutral penetration. For $\Delta\iota(s) = -0.2$ [curves labeled (a) in Fig. 13], the same cross section shows a square shape, so now the plasma is confronted with the problem of how to fit within the given bullet shape of the first-wall PFC boundary at $v = 0.5$—a square peg in a round hole problem! For the above reasons, one must expect that the range of achievable $\Delta\iota(s)$ depends on the details of the baseline plasma.

V.B. Variation of $\iota(s)$ at Fixed $\iota(0)$—Changing the Shear

Figure 14 and Table XIII show results from a similar calculation, where coil currents are adjusted so that the axis value $\iota(0)$ remains fixed at the nominal value $\iota(0) = 0.40$ and the edge iota is increased/decreased from the nominal value of $\iota(1) = 0.65$, thereby inducing a change in shear. The plasma current, toroidal field, plasma profiles, and β are held fixed so that the plasma contribution to iota, $\iota_p(s)$, remains essentially constant. Any change in $\iota(s)$ is due to the induced change in the external transform $\iota_{ext}(s)$.

The range of shear accommodated by the coils is $\int = (\iota_{\max} - \iota(0))/s_m = 0.23 \rightarrow 0.53$, where s_m is the value of scaled toroidal flux s at which ι is maximum. The ability to reduce the shear relative to the chosen baseline plasma is seen to be quite modest. The main impediment to shear reduction is the first-wall boundary location. Configurations with lower shear have been produced by the M45 coils, but they tend to overlap the first-wall boundary near the top/bottom of the inboard major radius (e.g., see limiting plasmas at $v = 0$ and $v = 0.25$ cross sections in Fig. 14).

The results in this section demonstrate a substantial capability for the M45 coil set to change the iota profile for fixed I_p, B_T, plasma profiles, and β. We have found similar flexibility to change the $\iota(s)$ profile for S1 states with $I_p = 0$ kA, a flexibility that is used to control $\iota(s)$ in the high-iota start-up scenario presented in Ref. 7.

VI. FLEXIBILITY TO STUDY KINK STABILIZATION BY 3-D SHAPING

The free-boundary I_p-β scan numerical experiments presented in Sec. III and summarized in Table V can be

TABLE X

Stability Properties and Effective Helical Ripple ε_h at $s = 0.3$, 0.5, and 0.8 for Pressure Profiles Parameterized by Peakedness Parameter γ [See Eq. (3) and Fig. 11]*

γ					
0.0	0.2	0.4	0.6	0.8	1.0
Kink: S Balloon: S ε_h (%) = 0.19 0.40 1.04	Kink: S Balloon: S ε_h (%) = 0.19 0.40 1.01	Kink: S Balloon: S ε_h (%) = 0.21 0.43 1.04	Kink: S Balloon: S ε_h (%) = 0.23 0.43 1.06	Kink: S Balloon: S ε_h (%) = 0.23 0.40 0.92	Kink: U Balloon: U on surfaces 2,3 only

*All equilibria correspond to $I_p = 174$ kA, $\beta = 3.0\%$, with $B_T = 1.7$ T at $R = 1.4$ m. The stable range of γ is $0 \leq \gamma \leq 0.8$. All equilibria correspond to $\beta = 3.0\%$.

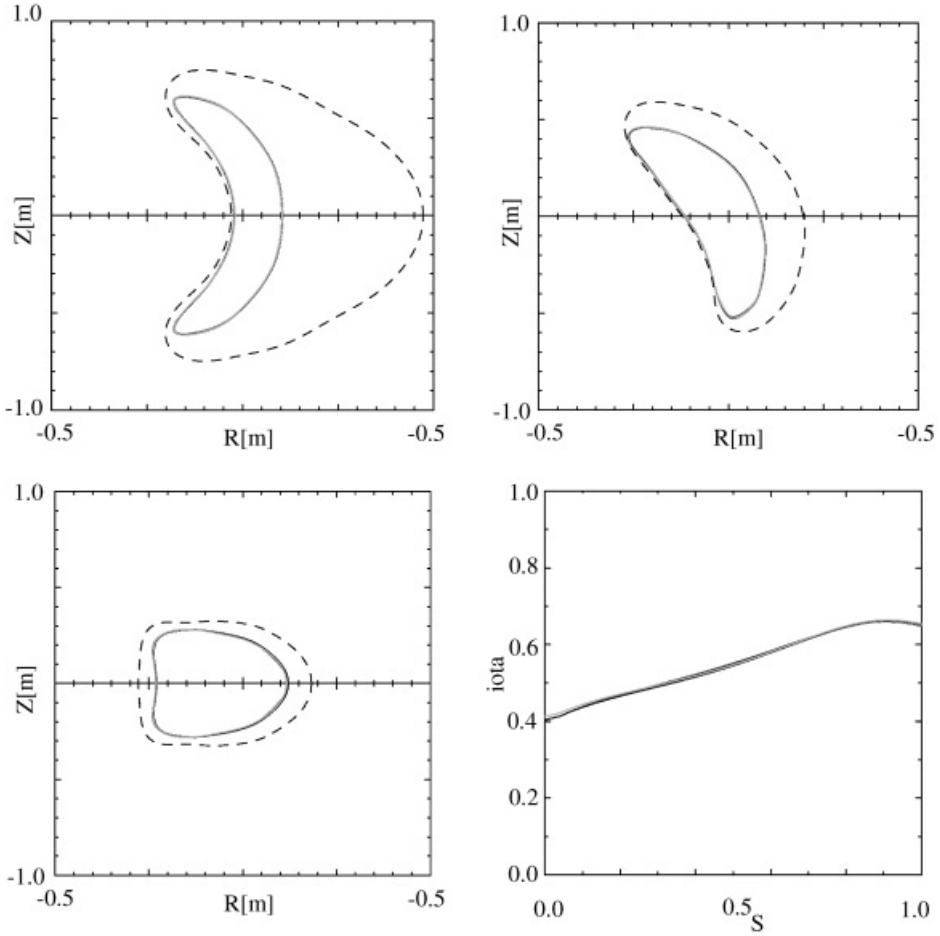

Fig. 12. Overlay of plasma boundaries and iota profiles for stable optimized configurations of the pressure profile scan ($\gamma = 0.0$, 0.2, 0.4, 0.6, and 0.8). $I_p = 174$ kA, $\beta = 3.0\%$ for all cases. Little change in shape is seen.

used to demonstrate the effect of MHD stabilization by 3-D shaping and to suggest controlled experiments to explore stability boundaries in NCSX.

Consider two configurations obtained by STELLOPT using the heavyside cost function measure of stability that have the same value of plasma current but different values of beta, for example, configurations with $I_p = 44.0$ kA, $\beta = 1.0\%$ and $I_p = 44.0$ kA, $\beta = 3.0\%$. As discussed in Sec. II, any stable "final state" of the optimizer using the heavyside feature is a state of marginal stability. Each plasma is at the β limit for its given shape and profiles; the plasma profiles are the same, yet the plasma shapes are quite different (see Fig. 15). Axis and edge iota values are $\iota(0) = 0.42$, $\iota(1) = 0.52$ for

TABLE XI

Coil Current Variation for the Pressure Profile Scans*

ΔI_{M1} (kA-turns)	ΔI_{M2} (kA-turns)	ΔI_{M3} (kA-turns)	ΔI_{TF} (kA-turns)	ΔI_{PF3} (kA-turns)	ΔI_{PF4} (kA-turns)	ΔI_{PF5} (kA-turns)	ΔI_{PF6} (kA-turns)
+17 −3	+19 −3	+12 −14	+3 −9	+0 −0	+4 −308	+6 −32	+3 −0

*In each column is shown the maximum +/− variation in the current for coil k compared with the current required to support the $\gamma = 0$ state.

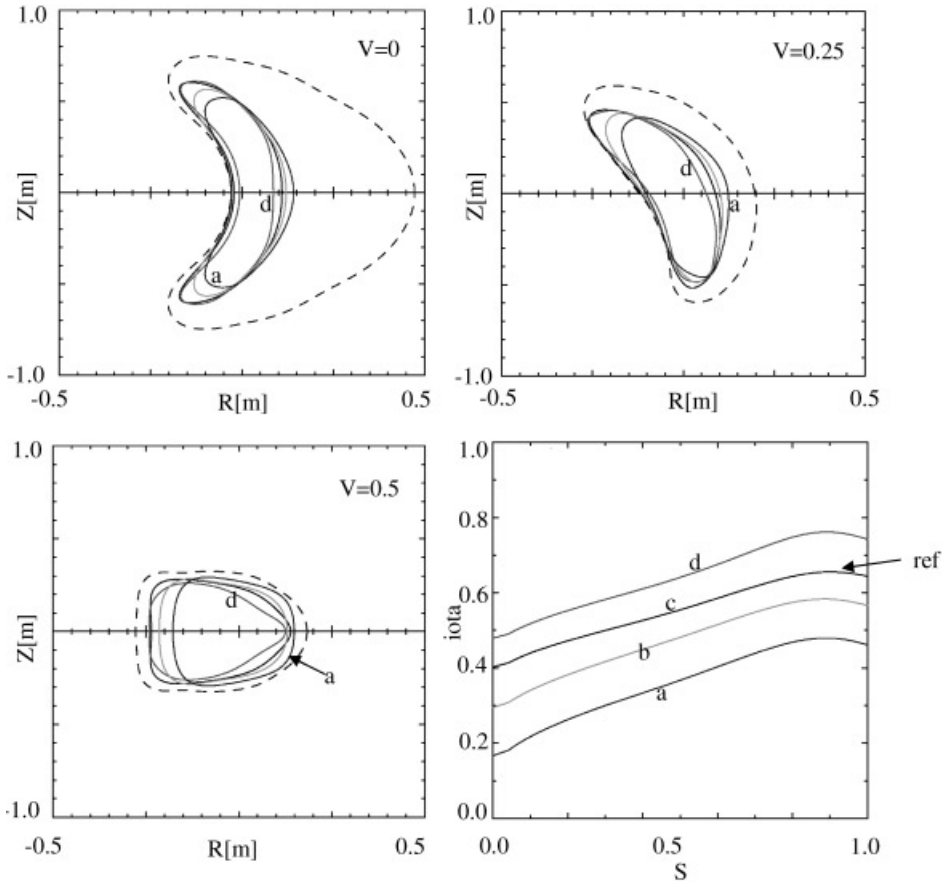

Fig. 13. Plasma boundaries and iota profiles for iota scan flexibility studies where coil currents are asked to change in such a way as to induce specified changes in $\iota(s)$. Here $\iota(s)$ is raised/lowered in such a way that the shear is preserved.

$I_p = 44.0$ kA, $\beta = 1.0\%$ and $\iota(0) = 0.41$, $\iota(1) = 0.46$ for $I_p = 44.0$ kA, $\beta = 3.0\%$.

Now consider the effect of taking the $I_p = 44.0$ kA, $\beta = 1.0\%$ configuration and raising β to 3.0% *while keeping the plasma boundary fixed*. The iota profile for this $\beta = 3.0\%$ "virtual" configuration is found to have $\iota(0) = 0.42$, $\iota(1) = 0.51$, little changed from the free-boundary 1.0% configuration. However, the $n = 1$ family of external kink modes is now strongly unstable as a result of the increase in β, with maximum eigenvalue $\lambda_1^K = -6.01 \times 10^{-4}$. Ballooning modes are also found over the split range of magnetic surfaces from $s = 0.31$ to 0.50 and from $s = 0.86$ to 0.96. It follows that the change in shape and the change in external transform associated with the change in coil current between the $I_p = 44.0$ kA, $\beta = 1.0\%$ free-boundary configuration and the $I_p = 44.0$ kA, $\beta = 3.0\%$ free-boundary configuration are responsible for the stabilization of the higher β

TABLE XII

Coil Current Variation for Raising/Lowering $\iota(s)$ at Constant Shear (See Fig. 13)*

$\Delta\iota$ (s)	ΔI_{M1} (kA-turns)	ΔI_{M2} (kA-turns)	ΔI_{M3} (kA-turns)	ΔI_{TF} (kA-turns)	ΔI_{PF3} (kA-turns)	ΔI_{PF4} (kA-turns)	ΔI_{PF5} (kA-turns)	ΔI_{PF6} (kA-turns)
+0.1	+65	+60	+75	−67	0	−1021	+113	+1
−0.1	−78	−61	−66	+73	0	−393	−33	+0
−0.2	−181	−157	−161	+167	−1684	−947	−40	+7

*Current differences are from the reference S3 state.

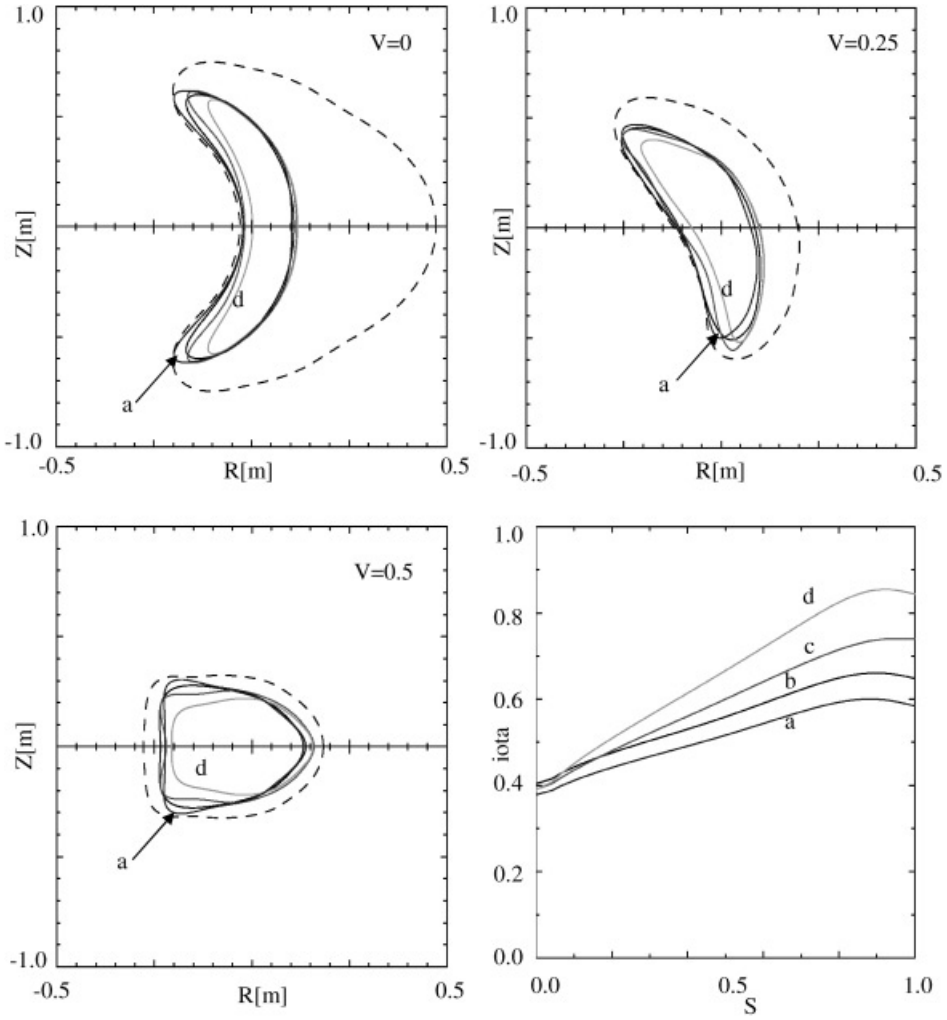

Fig. 14. Plasma boundaries and iota profiles for iota scan flexibility studies where coil currents are asked to change in such a way as to induce specified changes in $\iota(s)$. Here the shear is increased/decreased.

configuration; without this change of shape we would have obtained the unstable "virtual" configuration.

We have remarked that the $\iota(s)$ profile for the $I_p = 44.0$ kA, $\beta = 1.0\%$ free-boundary configuration has $\iota(1) = 0.52$. The question naturally arises whether the reduced β limit of this configuration compared with the $I_p = 44.0$ kA, $\beta = 3.0\%$ free-boundary configuration, which had $\iota(1) = 0.46$, is due to the destabilizing influence of the $\iota(1) = 1/2$ rational surface. The flexibility of the NCSX modular coil set to change the iota profile (demonstrated in Sec. V) can be used to test such a question. The free-boundary optimizer was rerun for the case

TABLE XIII

Coil Currents for Decreasing/Increasing Shear (See Fig. 14)

$\Delta\iota$ (1)	ΔI_{M1} (kA-turns)	ΔI_{M2} (kA-turns)	ΔI_{M3} (kA-turns)	ΔI_{TF} (kA-turns)	ΔI_{PF3} (kA-turns)	ΔI_{PF4} (kA-turns)	ΔI_{PF5} (kA-turns)	ΔI_{PF6} (kA-turns)
−0.07	−218	+309	−139	+15	0	−1161	+68	+0
+0.1	+40	+20	−13	−19	0	−617	−35	+0
+0.2	+64	+1	+17	−29	0	−1219	−94	−2

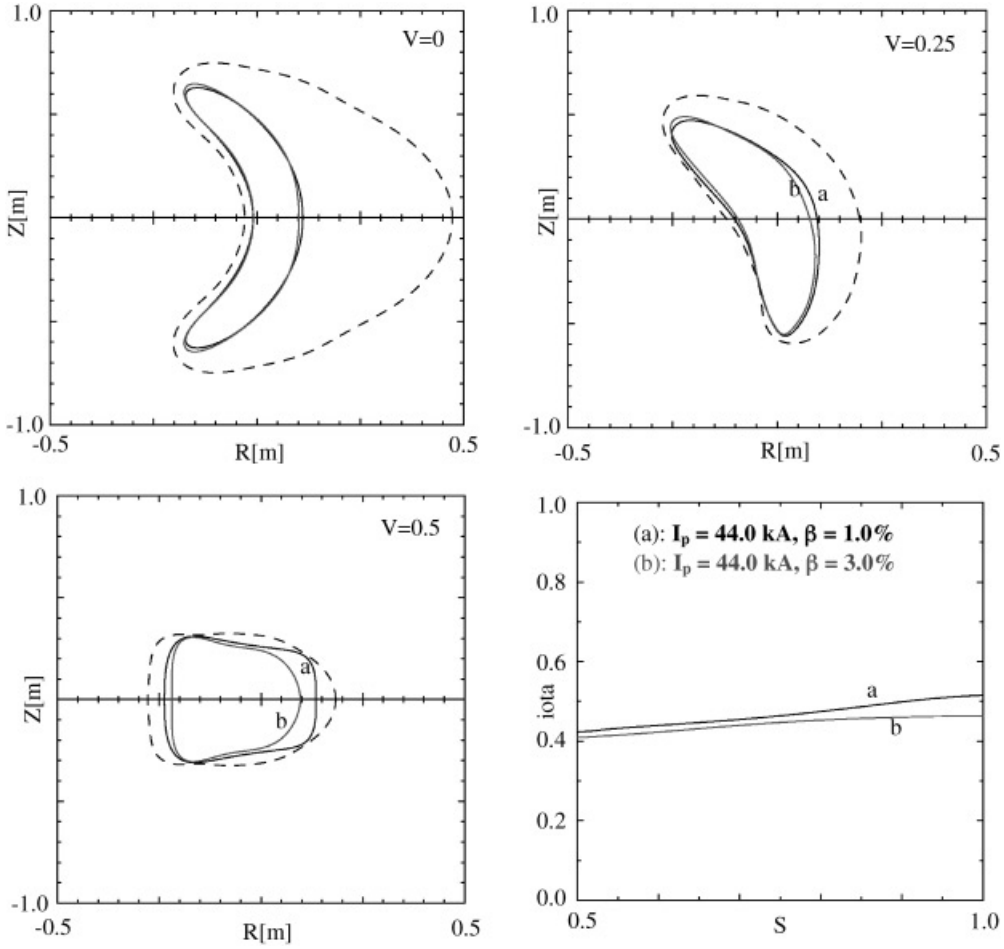

Fig. 15. Overlay of plasma boundaries and iota profiles for (a) $I_p = 44.0$ kA, $\beta = 1.0\%$ and (b) $I_p = 44.0$ kA, $\beta = 3.0\%$ used to illustrate MHD stabilization by 3-D shaping. Each configuration is at the β limit for its given shape and profiles. Profiles are the same for the two configurations, suggesting that the possibility that the enhanced β limit of the 3% configuration is due to the difference in shape. However, the iota profiles are different for the two configurations, and one needs to show that the difference in β limit is not due to an artificially low limit for the 1% configuration because $\iota = 0.5$ is in the edge region of the plasma.

$I_p = 44.0$ kA, $\beta = 1.0\%$ with the additional STELLOPT constraint that the coil currents produce a plasma shape with $\iota(1) = 0.46$ so that the $\iota = 0.5$ surface is no longer in the plasma region. A successful solution was found with $\iota(0) = 0.35$, $\iota(1) = 0.47$. The coil currents for this modified configuration are shown in the third row of Table XIV. Overlays of the modified $I_p = 44.0$ kA, $\beta = 1.0\%$ low-β-limit configuration and the marginally stable $I_p = 44.0$ kA, $\beta = 3.0\%$ configuration as well as the calculated $\iota(s)$ profiles are shown in Fig. 16. Stabilization at the enhanced β is now clearly due to 3-D shaping.

The ability to investigate the stabilizing role of 3-D shaping is an important element of the experimental program of NCSX. Investigations of this type allow testing and investigation of the stability boundaries of NCSX at low β.

VII. FLEXIBILITY TO VARY THE DEGREE OF QUASI-AXISYMMETRY

The ability to generate configurations with good quasi-axisymmetry is an essential requirement of the NCSX design. For a systematic exploration of the role of quasi-axisymmetry in improving the transport properties of stellarator plasmas, it is necessary to have the ability to control the degree of QA-ness. In this section we demonstrate this ability by varying NCSX modular coil currents to induce plasma shape changes that degrade/enhance the QA-ness (measured by the magnitude of the ripple amplitude ε_h) while maintaining plasma stability to kink and ballooning modes.

Figure 17 shows an overlay of plasma boundaries for three configurations, each with $I_p = 87.5$ kA, $\beta = 2.0\%$,

TABLE XIV

Coil Currents for Cases Illustrating MHD Stabilization by 3-D Shaping*

	M1 (kA-turns)	M2 (kA-turns)	M3 (kA-turns)	TF (kA-turns)	PF3 (kA-turns)	PF4 (kA-turns)	PF5 (kA-turns)	PF6 (kA-turns)
I_p: 44.0 kA β: 1.0% $\iota(0)$: 0.42 $\iota(1)$: 0.52	827.1	776.8	380.0	−0.4	−1.4	+7.5	−0.0	+0.0
I_p: 44.0 kA β: 3.0% $\iota(0)$: 0.41 $\iota(1)$: 0.46	733.6	700.4	593.7	−13.0	−166.7	+134.7	+80.2	+0.4
I_p: 44.0 kA β: 1.0% $\iota(0)$: 0.35 $\iota(1)$: 0.47	659.9	670.0	655.7	−0.7	−1.4	+5.8	−0.1	+0.0

*The three configurations are labeled (a), (b), and (c) in Figs. 15 and 16.

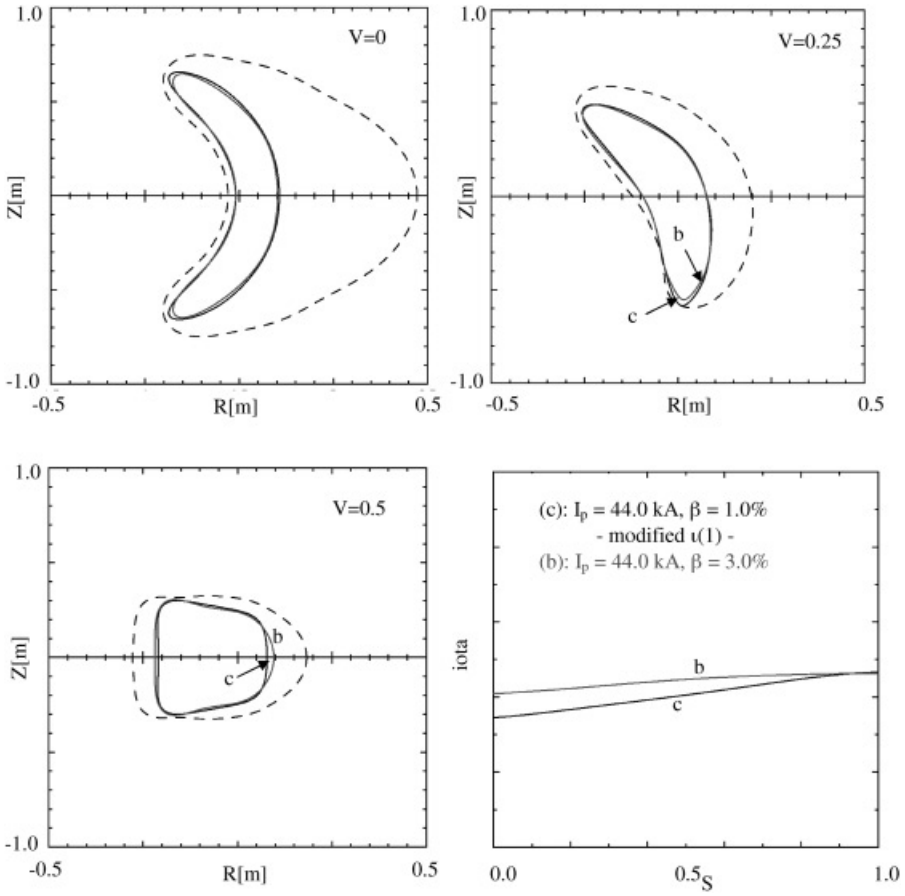

Fig. 16. Iota profile of the I_p = 44.0 kA, β = 1.0% configuration [(a) in Fig. 15] is modified by 3-D shaping [becoming configuration (c)] so that the edge iota is lowered to equal that of the I_p = 44.0 kA, β = 3.0% configuration (see Fig. 15). The ι = 0.5 surface now lies outside the plasma, showing that the β limit of the β = 1% configuration differs from that of the β = 3% configuration due to a difference in shape, not the proximity of $\iota(1)$ to 0.5.

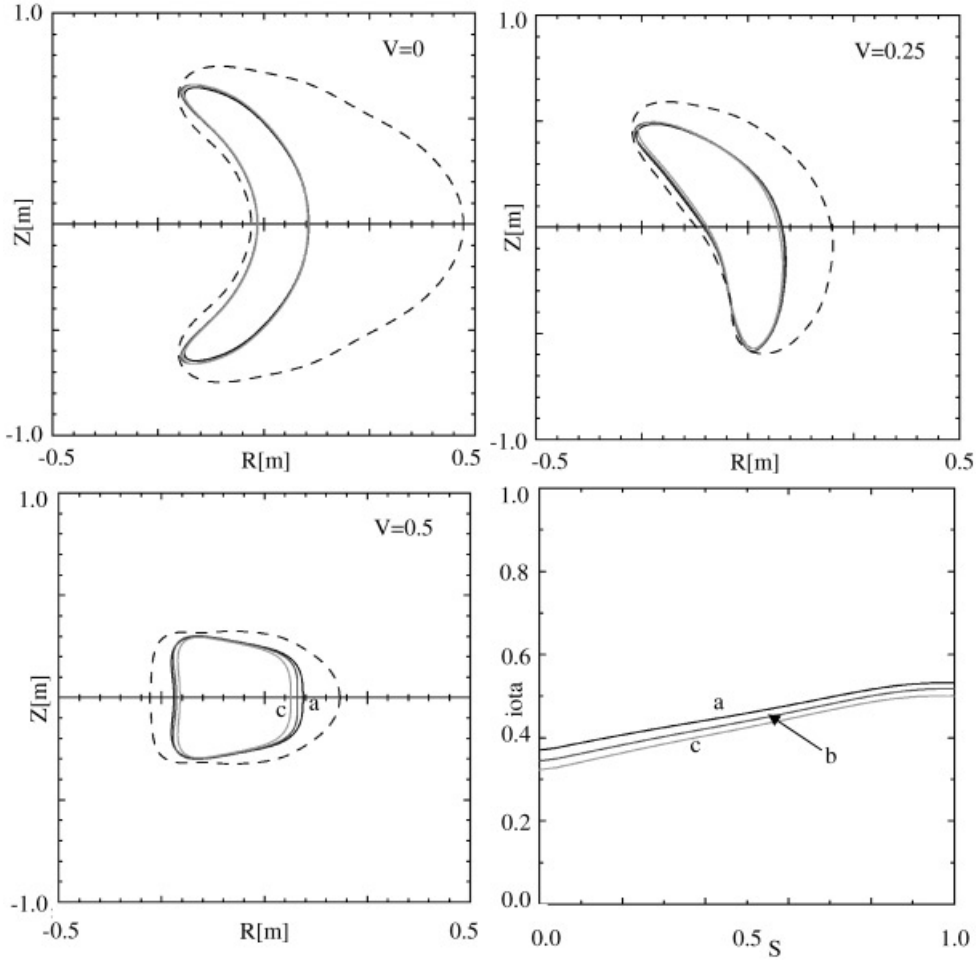

Fig. 17. Overlay of plasma boundaries for three configurations with $I_p = 87.5$ kA, $\beta = 2.0\%$, the same profiles of plasma current and pressure but different levels of quasi-axisymmetry (see Table XV). Each configuration is stable to kink and ballooning modes.

each with the same profiles of plasma current and pressure, but each exhibiting different degrees of quasi-axisymmetry. The ripple amplitude ε_h varies by a factor of 14 at the $s = 0.3$ surface, by a factor of 8 at $s = 0.5$, and by a factor of 4 at $s = 0.8$ (see Fig. 18). Coil currents that were required to support the equilibria are presented in Table XV. Each configuration is stable to kink and ballooning modes and was obtained using the free-boundary optimizer.

VIII. SUMMARY

We have presented a number of numerical experiments that demonstrate the ability of NCSX coils to meet the NCSX project mission. We have shown the following:

1. The NCSX plasma shape/position is robust with respect to uncertainties in the match between plasma profiles and assumed coil currents (see Table IV).

TABLE XV

Difference in Coil Currents Between High-ε_h Configuration (c) and Optimized ε_h Case (a) Shown in Figs. 17 and 18

ΔI_{M1} (kA-turns)	ΔI_{M2} (kA-turns)	ΔI_{M3} (kA-turns)	ΔI_{TF} (kA-turns)	ΔI_{PF3} (kA-turns)	ΔI_{PF4} (kA-turns)	ΔI_{PF5} (kA-turns)	ΔI_{PF6} (kA-turns)
−111	−38	+145	+0	+0	−7	−2	+0

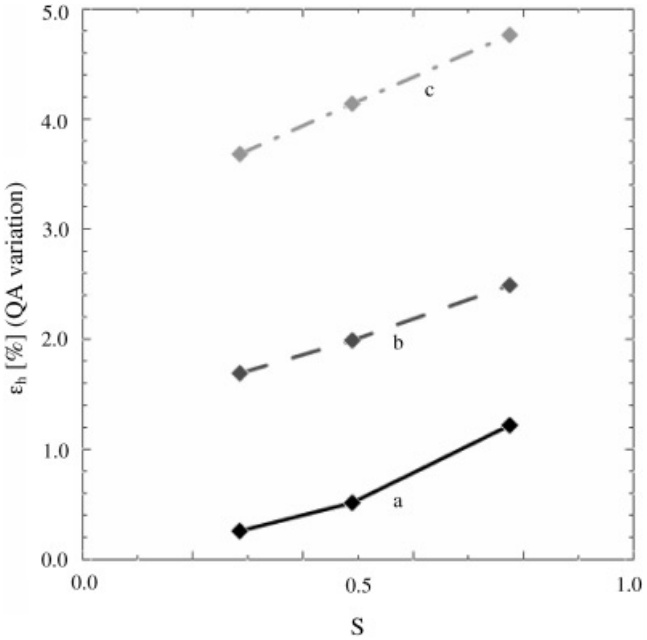

Fig. 18. Values of ε_h (%) as a function of toroidal flux for three configurations, each with I_p = 87.5 kA, β = 2.0%, each using the same profiles of plasma current and pressure, and each stable to kink and ballooning modes. Curve labeling is consistent with Fig. 17. The configuration corresponding to the black curve was originally obtained as part of the I_p-β scan discussed in Sec. III and presented in Tables IV and V.

2. Using reference M45 S3 plasma profiles, there is a wide operating space of I_p, β values for which plasmas supported by NCSX coils are stable to kink and ballooning modes and have low helical ripple amplitude ε_h (see Table V).

3. NCSX plasma performance is robust with respect to substantial variations in plasma current and pressure profile shape (see Tables VII and IX and the discussion of finite edge current in Sec. IV.B).

4. Substantial changes in the external transform $\iota(s)$ and shear $\iota'(s)$ can be induced by varying currents in the NCSX coils (see Tables XII and XIII and corresponding Figs. 13 and 14). This provides a significant control knob for the experimental determination of stable/unstable operating boundaries and the investigation of 3-D shape stabilization; see Sec. VI.

5. NCSX coils have the flexibility to control the degree of quasi-axisymmetry, allowing exploration of the physics of QA plasmas; see Sec. VII.

A subset of the calculations reported in this paper were duplicated using a related coil set named M45h. The M45h "healed" coils upon which the as-built NCSX modular coils are based are a subtle but important perturbation of the M45 coils, with superior flux surface quality. It was found that the M45 coil currents, when used as coil currents in the M45h healed coils, produce essentially identical stable configurations with the same quality of quasi-axisymmetry for states at the corners of flexibility space (the S1, S2, and S3 states in the I_p-β scans and states with $\alpha = 0.5$ in the current profile scans and $\gamma = 0.8$ in the pressure profile scans). This was to be expected since the healing of resonant fields that led from M45 to M45h (Ref. 13) required only minor deformations of the M45 coils, and hence minor changes in the equilibrium fields produced by these coils.

ACKNOWLEDGMENT

This work is supported by the U.S. Department of Energy, contract DE-AC02-76CH03073.

REFERENCES

1. D. STRICKLER et al., "Integrated Plasma and Coil Optimization for Compact Stellarators," *Proc. 19th IAEA Fusion Energy Conf.*, Lyon, France, Paper FT/P2-06 (2002).

2. S. P. HIRSHMAN and J. C. WHITSON, "Steepest-Descent Moment Method for 3D Magnetohydrodynamic Equilibria," *Phys. Fluids*, **26**, 3553 (1983).

3. D. V. ANDERSON, A. COOPER, U. SCHWENN, and R. GRUBER, *Proc. Joint Varenna-Lausanne Int. Workshop on Theory of Fusion Plasmas*, p. 93, Editrice Compositori, Bologna, Italy (1988).

4. R. SANCHEZ, S. P. HIRSHMAN, J. C. WHITSON, and A. S. WARE, "COBRA: An Optimized Code for Fast Analysis of Ideal Ballooning Stability of 3D Magnetic Equilibria," *J. Comput. Phys.*, **161**, 576 (2000).

5. V. V. NEMOV, S. V. KASILOV, W. KERNBICHLER, and M. F. HEYN, "Evaluation of $1/\nu$ Neoclassical Transport in Stellarators," *Phys. Plasmas*, **6**, 4622 (1999).

6. M. C. ZARNSTORFF et al., "Physics of the Compact Advanced Stellarator NCSX," *Plasma Phys. Control. Fusion*, **43**, A237 (2001).

7. E. A. LAZARUS et al., "Simulation of a Discharge for the NCSX Stellarator," *Fusion Sci. Technol.*, **46**, 209 (2004).

8. D. R. MIKKELSEN et al., "Assessment of Transport in NCSX," *Fusion Sci. Technol.*, **51**, 166 (2007).

9. M. I. MIKHAILOV and V. D. SHAFRANOV, "Stable Current Profile in a Stellarator with Shear," *Nucl. Fusion*, **30**, 413 (1990).

10. G.-Y. FU et al., "Ideal Magnetohydrodynamic Stability of NCSX," *Fusion Sci. Technol.*, **51**, 218 (2007).

11. D. MIKKELSEN, Personal Communication (2001).

12. R. JAENICKE, "Operational Boundaries on the Stellarator W7-AS at the Beginning of the Divertor Experiments," *Proc. 18th IAEA Fusion Energy Conf.*, Sorrento, Italy, October 4–10, 2000, Paper CN-77/OV4/3, International Atomic Energy Agency, Vienna, Austria (2000).

13. S. R. HUDSON et al., "Constructing Integrable High-Pressure Full-Current Free-Boundary Stellarator Magnethydrodynamic Equilibrium Solutions," *Nucl. Fusion*, **43**, 1040 (2003).